The Abdus Salam
International Centre for Theoretical Physics

United Nations
Educational, Scientific and
Cultural Organization

IAEA
International Atomic Energy Agency

**1864-28**

# Ninth Workshop on Non-linear Dynamics and Earthquake Predictions

***1 - 13 October 2007***

## Block Structure Modeling of Seismicity & Geodynamics in Italian Seismoactive Region: Application in Different Space Scale

Iness Vorobieva
*International Institute of Earthquake Prediction Theory & Mathematical Geophysics*
*Moscow, Russia*

# BLOCK STRUCTURE MODELING OF SEISMISITY AND GEODYNAMICS IN ITALIAN SEISMOACTIVE REGION: APPLICATION IN DIFFERENT SPACE SCALE

**Inessa Vorobieva**

# I. Modeling in the regional scale

The numerical block model of the lithosphere dynamics is used to simulate seismicity in the Italian area and its surroundings, based on the available structural and geodynamics information. The purpose of the study is to understand which are the tectonic processes that control the main features of the observed seismicity and the kinematics of the region. The influence of the rheology of the fault systems is studied as well.

## 1. Introduction

Earthquakes occur as a result of different processes, that are still not entirely described and understood. A possible approach to overcome the difficulties in studying seismicity, which are caused by the absence of fundamental constitutive equations for the dynamics of the lithosphere and by the impossibility of direct measurements at depth, where the earthquakes originate, relies on the integration of the numerical modeling of the lithosphere dynamics with the phenomenology of earthquake occurrence.

The block model described in detail by Soloviev and Ismail-Zadeh (2003) provides a straightforward tool for a broad range of problems, like the study of the dependence of seismicity on the general properties of the fault networks and rheology and the formulation and testing of different hypothesis for earthquake forecasting purposes. This is made possible by introducing some simplifications, the basic one being the assumption that the blocks are perfectly rigid. This assumption is justified by the fact that in the lithosphere the effective elastic moduli of the fault zones are significantly smaller than the ones within the blocks and it is rather realistic for short (as compared with the geological history) periods of simulation (thousands of years).

The method allows us to use a realistic geometry of the blocks, based on any relevant information. Driving tectonic forces (velocities of the boundary blocks and underlying medium) can be prescribed using geodetic data (GPS, VLBI), and the rheology of fault zones (parameters reflecting elasticity and viscosity) can be taken into account, as well, using the knowledge about the lithosphere structure, in terms of geometries and velocities of seismic waves propagation, and heat flow data. The output of the modeling consists of kinematical data on the block movements, that can be compared with observations (e.g. GPS), as well as of a synthetic earthquake catalog, where each event has origin time, coordinates of epicenter, magnitude and source mechanism. The synthetic earthquake catalog reproduces not only some of the basic global features of observed seismicity like (a) the Gutenberg-Richter law (e.g., Panza et al., 1997), (b) the space and time clustering of earthquakes (Maksimov and Soloviev, 1999) and (c) the dependence of the occurrence of large earthquakes on the fragmentation of the faults network, and on the rotation of blocks (Keilis-Borok et al., 1997), but also several regional features of seismicity, like (1) the epicenter distribution, (2) the relative level of seismic activity in different areas of the region and (3) the type of fault plane solution.

In this study, we consider a region covering Italy and surroundings. The purpose of the study is to understand what tectonic processes control the features of the observed seismicity and the kinematics of the region, as well as the influence of the rheology of the fault system on the seismicity. The block structure has been outlined on the basis of the seismotectonic model developed by Meletti et al. (2000) and of the space distribution of seismicity. The idea to represent this region as a system of perfectly rigid blocks is supported by the existence of some

large, almost aseismic territories, like the Adria micro-plate. The area of active deformation along the Apennines, in the present study, is simplified: Apennines are represented by blocks bounded by a system of parallel faults, which are assumed to represent as a whole the complex system of small faults. To estimate the quality of the modeling, the results of the numerical simulation are compared with the observations. Specifically, the block motions are qualitatively checked against geodetic observations (GPS and VLBI), while the epicenter distribution, the location of the largest events, the type of source mechanisms and the slope of the Gutenberg-Richter law for the synthetic seismicity are compared with the observed ones.

## 2. Geodynamics and block structure for the Italian region and its surroundings

Different criteria can be followed to define the geometry of the block structure, which depends from the main geological elements of the region as well as the scale and detail of the model. In some previous studies the morphostructural zonation of the study region, e.g. the Western Alps (Cisternas et al., 1985), has been used as the base for the block structure geometry (Vorobieva et al., 2000; Soloviev and Ismail-Zadeh, 2003). In the present work, which is performed on a larger space scale, we use as a base the seismotectonic model of the study area (Scandone et al., 1990, 1994, Meletti at al., 2000) and the space distribution of observed seismicity.

According to Meletti et al. (1995, 2000), the recent geodynamics of the Central Mediterranean region is controlled by the Africa-Europe plate interaction and by the passive subduction of the south-western margin of the Adria plate. The main regional geological features observed in Italy and surroundings are represented by the Alps, by the back-arc Tyrrhenian extensional basin, by the Apennines and by the Padan-Adriatic-Ionic foreland.

Apennines, Alps and Dinarides outline the western, northern and eastern boundaries of the Adria respectively, while the location of the southern boundary is still controversial. A counter-clockwise rotation of the Adria seems to justify the main characteristics, both structural and kinematics, of its boundary regions (Anderson and Jackson, 1987; Ward, 1994). The evolution of the Apennines, however, does not seem to be explained by a simple convergence process and some evidences suggest that it might be controlled by passive subduction processes (Meletti et al., 1995; Pasquale et al., 1997; Doglioni, 1991; Doglioni et al., 1999a).

A band with tensional seismotectonic behavior, with prevailing dip-slip focal mechanism, characterizes the northern part of the Italian peninsula, from the Po plain to the Ortona-Roccamonfina line. Two belts run parallel to it: the western one is composed by the tensile zones near to the Tyrrhenian coast and the eastern one by the contraction zones along the Adriatic Sea.

The subduction of the Adriatic foreland in the Southern Apennines, from the Ortona-Roccamonfina line to the Taranto Gulf, seems to be ceased, while a passive subduction continues in the concave part of the Calabrian Arc, where a zone of active seismicity is identified, immerging toward the Tyrrhenian basin and reaching a depth of about 500 km (Caputo et al., 1970, 1972; Anderson and Jackson, 1987; Panza et al., 2003).

As concerning the Adria plate, it remains still unclear if it is connected to the Africa plate or if it moves as an independent plate, since neither a structural nor a seismically active boundary between the Adria and Africa plate is clearly evidenced. At the same time the movements of the Adria and Africa plates appear quite different: the stress distribution appears compatible with a counter-clockwise rotation of the Adria, with respect to Eurasia, with a rotation pole well distinguished from that proposed for the Africa-Eurasia rotation.

The block structure we outlined for the dynamical modeling of seismicity in the Italian region is based on the main features of observed seismicity, and takes into account the geodynamic, structural and seismotectonic framework just discussed, in agreement with the sketch proposed by Meletti et al., (2000). The configuration of its faults, on the upper plane, is shown in Figure 1.1. Since one of the aims of the model is to reproduce the main features of the space distribution of observed seismicity (Figure 1.2), the modeled faults have to be introduced in the structure corresponding to the most seismically active areas and fault zones.

The block structure consists of eleven blocks. These blocks are contoured by 36 faults that are marked in Figure 1.1 from I to XI and from 1 to 36, respectively.

Two main longitudinal discontinuities (faults 25 - 29) have been placed along the North-Central Apennines, to model the Adriatic contraction front and the extension belt. Fault 8 has been placed, corresponding to the Ortona-Roccamonfina line (Meletti et al., 2000), while faults 30 and 32 have been placed south of it to model the seismic activity from Irpinia to the Pollino, along the Southern Apennines. A possible discontinuity (fault 11) is assumed to exist between Adria and Africa plates, south of Apulia; an almost EW oriented discontinuity (fault 33) has been placed according to the observed seismicity, crossing the Gargano and the Adria plate from the Apenninic chain up to the Dinarides. Battaglia et al. (2004) also assume a similar boundary, dividing Adria into two subplates separated by the Gargano-Dubrovnik fault, in agreement with the parametric studies by Oldow et al. (2002). Nine boundary blocks, which are marked as BB1 - BB9 in Figure 1.1, are introduced to specify the motion of the confining medium at the lateral boundaries of the structure.

To choose the value of the thickness $H$ of the layer $d$ we analyze the distribution of the hypocenters of observed seismicity. Most of them are within 30 km depth. Another reason to specify $H$ = 30 km is given by the recent data on the deep structure of Italy and surroundings. According to Chimera et al. (2003) and Panza et al. (2003), there is a rather extended lithospheric region where, at an average depth of about 30km, the S-wave velocity is rather low, with consequent decoupling between the upper and lower layers of the lithospheric mantle.

The dip angles of the faults have been specified on the basis of the source mechanisms of the observed earthquakes (Sarao' et al., 1997). The faults have been separated into two groups: near-vertical and oblique faults. The same value of the dip angle has been assigned to all the faults belonging to the same group: $85^o$ - for near-vertical faults, and $60^o$ - for oblique faults. The dip angle of each fault is indicated in Figure 1.1

The block structure thus defined and the above mentioned information have been the starting point for a wide set of numerical experiments described below, which permitted, step by step, to reproduce several relevant features of the observed kinematics and seismicity.

**3. Numerical Experiments**

The values of the parameters for the blocks and the faults and the movements specified for the underlying medium and the boundary blocks have been varied in a set of parametric experiments. We report here about the 5 experiments that we consider most significant.

The following set of values has been assumed as a benchmark and we call it, from now on, the "standard set". The medium underlying all the blocks and the boundary blocks BB1 - BB3 and BB6 - BB9 do not move. The boundary blocks BB4 and BB5 move progressively with the velocity $V_x$ = -25 cm, $V_y$ = 65 cm per unit of dimensionless time, respectively. This direction of velocity has been chosen according to NUVEL-1A model (Gripp and Gordon, 1990; DeMets et al., 1990; DeMets et al., 1994). For all blocks and faults the coefficients in (1) are: $K$ = 1 bar/cm and $W$ = 0.05 cm/bar. For all faults the thresholds for $\kappa$ are: $B$ =0.1, $H_f$ = 0.085, and $H_s$ = 0.07, and for $W_s$ = 5cm/bar, like those used in previous studies (i.e. Panza et al., 1997; Soloviev et al., 2000; Vorobieva et al., 2000). In all experiments the value of $P$ equals 2 Kbars, and the values of the parameters for the discretization, in time and space, are $\Delta t$ = 0.0001 units and $\varepsilon$ = 5 km, respectively.

In the first experiments we change step by step the movements of the underlying medium and of the boundary blocks taking into account the following main features of the geodynamics of the region:

- convergence of African and European plates;
- counterclockwise rotation of the Adria plate, with the pole of rotation in the Western Alps;
- opening of the Tyrrhenian basin.

The influence of the rheology is studied in the final stage of work.

The features of the observed seismicity, which follow from the analysis of the epicenter distribution and source mechanism, have been used to estimate the results of the experiments:

- two seismoactive belts in the north-central Apennines: the eastern one in contraction, the western one in extension;
- double extensional belt in the Southern Apennines;
- contractional belts along the Dinarides and the Southern Alps;
- absence of seismicity along the southern boundary of the structure, i.e. unknown boundary between Africa and Adria.

***Experiment 1***

*Purpose:* to check whether the convergence of Africa and Europe alone can explain the main features of tectonics and seismicity in the region.

*Values of the parameters:* the standard set given above in this section.

*Results:* Adria undergoes a counterclockwise rotation, but its northern part (block IV) moves NW, and not northward, as it should be to reproduce observations (Nocquet and Calais, 2003). Most of the synthetic seismicity is concentrated along the southern boundary of the structure, where observed seismicity is absent. Excluding two clusters of events in the Alps, the synthetic seismicity is absent in the northern part of the model where, on the contrary, the observed seismicity is considerable. The average velocities of the blocks are listed in Table 1.1, and the epicenters of the synthetic earthquakes are shown in Figure 1.3.

When only the movement of the boundary blocks representing the African plate is specified it is impossible to obtain the distribution of the synthetic epicenters and the directions of the block motions like those known from the observations.

***Experiment 2***

*Purpose:* to reproduce the direction of motion of the northern part of the Adria (block IV), and to improve the fit with observed seismicity, by removing the synthetic seismicity from the southern boundary of the block structure and by making seismically active its northern part. We introduce the movement of the Adria plate, simulating a rotation around the pole in the Western Alps (Meletti et al., 2000), with direction in agreement with the configuration of the mantle wedge proposed by Doglioni et al, (1999b).

*Values of the parameters:* The standard set is modified as follows. The translational velocities of the boundary block BB4 and of the underlying medium, for blocks IV - VIII and XI, correspond to a rotation of the Adria plate around the pole with geographical coordinates 44.2$^{o}$N and 8.3$^{o}$E (Meletti et al., 2000). This means that the prescribed velocities are orthogonal to the radius vector from the pole of rotation to the center of the block and that the values of the velocities are proportional to its distance from the pole of rotation (as given in Table 1.2). The velocity of the underlying medium for block X is the same as the velocity of the boundary block BB5, $V_x$ = -25 cm, $V_y$ = 65 cm per unit of dimensionless time.

*Results:* A counterclockwise rotational component of the movement for blocks IV and VI, representing the Adria plate, is obtained. The northern part of the Adria (block IV) moves northward. Extension along the double seismic belt in the Southern Apennines (faults 30, 32) and contraction along the Dinarides (faults 9, 10) are obtained, but the model does not reproduce the extension–contraction belt in the North-Central Apennines (faults 25 - 29). The southern boundary of the structure becomes aseismic, while the northern part of the structure is active till the Alps. High seismicity appears at the eastern edge of Sicily. A seismic belt appears in the Southern Apennines, but there is no synthetic seismicity at the western edge of the North-Central Apennines. The level of seismicity is not high enough in the Calabrian arc and in the Dinarides. The average velocities of the blocks are listed in Table 1.2 and the epicenters of the synthetic earthquakes are shown in Figure 1.4. The resulting movements of the blocks and synthetic seismicity become more similar to the observations than in Experiment 1. This fact can be

interpreted as a confirmation that the Adriatic plate is an independent microplate (Battaglia et al., 2004).

***Experiment 3***

*Purpose:* to reproduce the extension–contraction belt in the North-Central Apennines and to increase the level of seismic activity in the Calabrian arc. Experiment 3 is based on the assumption that the geodynamics of the region is controlled not only by the convergence of Africa and Eurasia, but also by the passive subduction of the south-western margin of the Ionian-Adria plate, which causes the opening of the Tyrrhenian basin (e.g. Pasquale et al., 1997).

*Values of the parameters:* with respect to the set of parameters considered in Experiment 2, the following changes are made: the velocities of the boundary block BB7 and of the underlying medium for block III are replaced respectively by $V_x$ = -30 cm, $V_y$ = 30 cm, and by $V_x$ = 55 cm, $V_y$ = 45 cm per unit of dimensionless time.

*Results:* The counterclockwise rotation of the Adria plate, the extension in the southern Apennines and the contraction along the Dinarides are mimed. The extension–contraction belts in the north-central Apennines are obtained as well. A high synthetic seismic activity appears along the western edge of the northern Apennines. The synthetic seismicity increases in the Calabrian arc, while it becomes comparatively too intense at the eastern edge of Sicily. The average velocities of the blocks are listed in Table 1.3 and the epicenters of the synthetic earthquakes are shown in Figure 1.5. The likelihood of tectonic motions and of synthetic epicenters distribution is improved considerably with respect to previous experiments, while the comparative levels of the synthetic seismicity, in the different parts of the structure, still are not in sufficient agreement with the observations.

***Experiment 4***

*Purpose:* to study how the synthetic seismicity depends on the coupling between the blocks and the underlying medium. We change the visco-elastic characteristics of the block bottoms in Calabria, Apennines and Alps

*Values of the parameters:* with respect to Experiment 3, $W$ is decreased for blocks I, III, V, VII, and XI to 0.005 cm/bar, and for block II to 0.015 cm/bar.

*Results:* The level of the synthetic seismicity increases slightly along the contraction belt in the North-Central Apennines and remains too high at the western edge of Sicily and in the extension belt of Northern Apennines. The average velocities of the blocks are listed in Table 1.4 and the epicenters of the synthetic earthquakes are shown in Figure 1.6. The synthetic seismicity raises in the contraction belt of the north-central Apennines and in the southern Apennines.

***Experiment 5***

*Purpose:* to decrease the synthetic seismicity along the extension belt in the northern Apennines and at the eastern edge of Sicily, and to increase it along the contraction belt in the north-central Apennines. We modify the parameters that define the visco-elastic characteristics of the faults along the eastern edge of Sicily

*Values of the parameters:* the following changes have been made, with respect to the set of parameters used in Experiment 5: for faults 25 - 27 (the eastern side of the north-central Apennines) the values of $W$ and $W_s$ are set equal to 0.005 and 0.5 cm/bar, respectively, and for faults 15, 28, and 29 (the eastern edge of Sicily and the western edge of Northern Apennines) the values of $W$ and $W_s$ are set equal to 0.5 and 50 cm/bar, respectively.

*Results:* The synthetic seismicity decreases at the western edge of the north-central Apennines and at the eastern edge of Sicily, while it increases in the southern Apennines. The average velocities of the blocks are listed in Table 1.5 and the epicenters of the synthetic earthquakes are shown in Figure 1.7. As a result the synthetic seismicity in the western edge of the north-central Apennines and in the eastern edge of Sicily decreases.

The 5th variant of the model qualitatively reproduces the basic features of the observed seismicity: mainly the epicenter distribution and the relative levels of seismicity in different parts of the region, and the overall tectonic motions in the study area. Therefore in the following we analyze quantitatively and discuss in detail the results of Experiment 5.

## 4. Analysis of the result

### *4.1 Block movements*

The numerical simulation of the block structure dynamics has been performed for a period of 20 units of dimensionless time. The resulting average velocities of the blocks are shown in Figure 1.8 by open arrows, while the black arrows indicate the motion inferred from the geodetic measurements (Devoti et al., 2002). Observed movements are available for the blocks III, IV, VI, X, XI. The movements obtained in the model exhibit a good agreement with these observations. The values of the average translational and angular velocities of the blocks of the structure are given in Table 1.6. All blocks move in the NE direction, except blocks I and X, which represent Western Alps and Sicily and move in the NW direction. The absolute values of velocities decrease going northward, and blocks I and II, representing the Alps, are almost motionless; this fact is in qualitative agreement with the results of Jimenez-Munt et al. (2003)

The counter-clockwise rotation of blocks IV and VI is in good agreement with the rotation of the Adria plate (Meletti et al., 2000). Comparing the resulting velocities of the blocks (Table 1.5 and Fig. 1.8) it is possible to observe that there is extension on faults 28, 29 30 and 32 in Figure 1.2, which represent the extension zone along the Apennines, and compression at the eastern edge of block III, which represents the contraction band, along the Adriatic Sea, in the North-Central Apennines. Contraction zones are formed along the eastern edge of blocks IV and VI (the boundary between Adria and Dinarides), and along the southern boundary of the Alps (fault 24 in Fig. 2.1); while an extension zone is obtained in the Calabrian Arc (faults 19 and 20 in Fig. 1.1). These results are in agreement with the stress map of Italy (Montone et al., 1999) and with the World Stress Map (Mueller et al., 2000).

### *4.2 Synthetic seismicity*

The magnitudes of the synthetic earthquakes range between 5.2, the minimum magnitude allowed by the specified value of ε (5 km), and 7.6. The distribution of the epicenters of the synthetic earthquakes is shown in Figure 1.7 and appears in rather good agreement with observed epicenters (Fig. 1.2).

The slope (*b*-value) of the frequency-magnitude (FM) plot (Fig. 1.9), or Gutenberg-Richter law, appears larger for the synthetic seismicity (1.44±0.07) than for the observed one (1.14±0.05). To draw the FM plot for the observed seismicity we consider only the period 1900-2000, as the Leydecker catalog is not complete for magnitude 5 before 1900. From the difference in the number of events with magnitude $M \geq 5$, it is possible to estimate that a dimensionless unit of time corresponds to about 1500 years, thus our experiments cover a time interval of about 30,000 years. The difference in the *b*-values obtained for observed and synthetic seismicity may be explained by the fact that the model does not reproduce with sufficient detail the fault network of the region under consideration.

Accordingly to the analysis performed by Molchan et al. (1997), the *b*-value calculated for the observed seismicity in Northern and Central Italy is essentially larger than that in Southern Italy (excluding Sicily). The *b*-values calculated for these regions, either considering the synthetic seismicity and the observed one catalog UCI2001 (Peresan and Panza 2002), exhibit a similar difference.

In the *North-Central Apennines* (faults 25, 26, 27, 28, and 29 in Fig. 1.1) the synthetic seismicity is modeled along two belts. In agreement with the observations the western belt is more active than the eastern one. The largest synthetic events (with $M$ = 6.8) occur nearby the junction between the Apennines and the Alps. Actually, some large events (e.g. the M=6.7 Garfagnana earthquake, occurred on September 1920), took place in the north-western part of the Apennines, corresponding to the location of fault 28, but the frequency observed for such events is not as high as that shown in Figure 1.2.

In the *Southern Apennines* (faults 30 and 32 in Fig. 1.1) the synthetic seismicity is represented along two belts as well, and the level of the synthetic seismicity is higher than in North-Central Apennines, in agreement with the observations. The maximum synthetic

magnitude equals 7.6. Here the largest observed earthquakes occurred in 1930 ($M$ = 7.5) and 1857 ($M$ = 7.0), and several events with $M \geq 6.5$ are reported.

In the *Calabrian arc* (faults 19 and 20 in Fig. 1.1) the level of the synthetic seismicity is high and the maximum synthetic magnitude is 7.3, not far from the value 7.1 of the largest observed earthquake (Messina, 1908).

At the *eastern edge of Adria* (faults 9 and 10 in Fig. 1.1), in the southern part of the Dinarides, the level of the synthetic seismicity, with a maximum synthetic magnitude 6.8, underestimates the observed seismicity, with maximum magnitude 7.5. The highest synthetic seismicity is obtained in the Northern Dinarides, where several synthetic earthquakes with magnitude $M \geq 7.5$ occur, the largest having $M$ = 7.6. The maximum magnitude observed here corresponds to the M = 7.9 earthquake occurred in 1348, in the vicinity of the conjunction of the Alps and the Dinarides.

At the *eastern edge of Sicily* (fault 15 in Fig. 1.1) the maximum synthetic magnitude is 7.2. The largest observed earthquake, with $M$ = 7.5, occurred along the Malta escarpment in 1693; several events with $M \geq 6.5$ are also reported for this fault zone.

In the *Southern Alps* (fault 24 in Fig. 1.1) the maximum synthetic magnitude is 6.6, and the largest observed earthquake, $M$ = 6.8, occurred in 1222.

### *4.3 Source mechanisms*

The source mechanisms of the synthetic earthquakes have been analyzed in different parts of the block model.

The available source mechanisms of the observed earthquakes (e.g. Saraò et al., 1997, Vannucci et al., 2004), are compared with the synthetic ones. We consider several sub-regions corresponding to different parts of the block structure and the observed fault plane solutions are divided into three groups: strike-slip (rake between $-30^o$ and $30^o$, or $-150^o$ and $150^o$), normal faulting (rake between $-30^o$ and $-150^o$), and reverse faulting (rake between $30^o$ and $150^o$). The results are presented in the Figure 1.10. As a whole, the comparison of the mechanisms obtained in the model with the observations and the stress map of Italy (Montone et al., 1999) shows a good agreement. Normal faulting is typical for the synthetic seismicity in the Apennines, the eastern edge of Sicily and the Calabrian arc, while reverse faulting predominates in the north-western boundary of the Adriatic Sea, in the Southern Alps and along the eastern edge of the Adria in Dinarides.

## 5. Conclusions

The results of the numerical simulation of lithosphere block structure dynamics show that it is possible to reproduce the main features of observed seismicity, which are mainly controlled by the motions prescribed in the model. Taking into account rheology allows adjust the relative levels of the seismic activity in the different territories.

The model permits to reproduce the main observed features of the tectonic motions as well. The movements obtained as a result of the numerical simulation exhibit a good agreement with the available observations (GPS and VLBI); the extension belt along the Apennines and the contraction belt along the north-western boundary of the Adriatic Sea are correctly reproduced.

The results of the modeling allow us to check some hypotheses about the tectonic processes controlling the geodynamics and seismicity in the study area. The main conclusion is that the available observations cannot be explained only as a consequence of the convergence of Africa and Europe. thus corroborating the results of previous studies, obtained using various geodynamical models. In particular, Bassi and Sabadini (1994) and Bassi et al. (1997) showed, by means of a thin-sheet viscous model, that subduction of the Ionian lithosphere underneath the Calabrian arc is necessary to explain the extensional style of the Tyrrhenian sea, and Jimenez-Munt et al. (2003), who used the thin-shell finite element approach to simulate active deformation in Mediterranean region, evidenced that the deformational style in the Mediterranean region is controlled by the Africa-Eurasia convergence and by the subduction in the Calabrian Arc and Aegean Sea.

The processes controlling the tectonics and the seismicity in the study region seem to be therefore quite complex. Introducing the rotation of the Adria plate around a rotation pole in the Western Alps, we obtain a relatively more credible movement of the block structure, and thus we indirectly support the hypothesis that the Adria is an independent, possibly fragmented (Oldow et al., 2002) microplate, compatibly with recent tomographic studies (Venisti et al, 2004). Battaglia et al., (2004) reached similar conclusion using GPS measurements and block modeling to study present-day deformations of the Adriatic region. At the same time some additional processes, connected with the passive subduction of the Ionian-Adria plate, seem to play a relevant role in the coexistence of contraction and extension belts in the North-Central Apennines (Frepoli and Amato, 1997) as well as in the high level of seismicity in the Calabrian Arc.

The influence of the geometries and level of detail of the model as well as of the structural properties of the studied region, as reflected by the different coupling of the blocks with the underlying medium and by the differences in the rheology of fault zones, will be subject of forthcoming investigations.

# References


Anderson, H., and Jackson, J. (1987), *Active tectonics in the Adriatic region*, Geophys. J. R. Astr. Soc. *91*, 937-983.

Bassi, G., and Sabadini, R. (1994), *The importance of subduction for the modern stress field in the Tyrrhenian area*. Geophys. Res. Lett. *21***,** 329-332.

Bassi, G., Sabadini, R., and Rebaï, S. (1997), *Modern Tectonic regime in the Tyrrhenian area: observations and models*, Geophys. J. Int. *129***,** 330-346.

Battaglia, M., Murray, M., Serpelloni, E., and Bürgmann, R. (2004), *The Adriatic region: An independent microplate within the Africa-Eurasia collision zone*, Geophys. Res. Lett. *31*, L09605, doi:10.1029/2004GL019723.

Caputo, M., Panza, G. F., and Postpischl, D. (1970), *Deep structure of the Mediterranean basin*, JGREA *75*, 4919.

Caputo, M., Panza, G. F., and Postpischl, D. (1972), *New evidence about the deep structure of the Lipari arc*, Tectonophysics *15*, 219.

Chimera, G., Aoudia, A., Saraò, A., and Panza, G. F. (2003), *Actives tectonics in Central Italy: constraints from surface wave tomography and source moment tensor inversion*, Phys. Earth Planet. Inter. *138*, 241-262.

Cisternas, A., Godefroy, P., Gvishiani, A., Gorshkov, A. I., Kosobokov, V., Lambert, M., Ranzman, E., Sallantin, J., Saldano, H., Soloviev, A., and Weber, C. (1985), *A dual approach to recognition of earthquake prone areas in the western Alps*, Annales Geophysicae *3*, 249-270.

Devoti, R., et al. (2002), *Geophysical interpretation of geodetic deformations in the Central Mediterranean area*. In *Plate Boundary Zones* (eds. Stein, S., and Freymueller, J. T.), Geodynam. Ser., vol. 30, pp. 57-65.

Doglioni, C. (1991), *A proposal of kinematic modeling for W-dipping subductions - Posible applicatons to the Tyrrhenian-Apennines system*, Terra Nova *3***,** 423-434

Doglioni, C., Gueguen, E., Harabaglia, P., and Mongelli, F. (1999a), *On the origin of west-directed subduction zones and application to the western Mediterranian*. In *The Mediterranean Basins: Tertiary Extension within the Alpine Orogen* (eds. Durand, B. *et al.*) (Geological Society, London) Special Publications, vol. 156, pp. 541-561.

Doglioni, C., Harabaglia, P., Merlini, S., Mongelli, F., Pecerillo, A., and Piromallo, C. (1999b), *Orogens and slabs vs. their direction of subduction*, Earth-Science Reviews *45***,** 167-208.

Jimenez-Munt, I., Sabadini, R., and Gardi, A. (2003), *Active deformation in the Mediterranean from Gibraltar to Anatolia inferred from numerical modeling and geodetic and seismological data*, J. Geophys. Res. *108* (B1), 1-24.

Keilis-Borok, V. I., Rotwain, I. M., and Soloviev, A. A. (1997), *Numerical modelling of block structure dynamics: dependence of a synthetic earthquake flow on the structure separateness and boundary movements*, J. Seismol. *1*, 151-160.

Maksimov, V. I., and Soloviev, A. A. (1999), *Clustering of earthquakes in a block model of lithosphere dynamics*. In *Computational Seismology and Geodynamics* (ed. Chowdhury, D. K.), vol. 4 (Am. Geophys. Union, Washington, D.C.) pp. 124-126.

Meletti, C., Patacca, E., and Scandone, P. (1995), *Il sistema compressione-distensione in Appennino.* In *Cinquanta anni di attività didattica e scientifica del Prof. Felice Ippolito* (eds. Bonardi, G. *et al.*) (Liguori, Napoli) pp. 361-370.

Meletti, C., Patacca, E., and Scandone, P. (2000), *Construction of a seismotectonic model: the case of Italy*, Pure Appl. Geophys. *157*, 11-35.

Molchan, G., Kronrod, T., and Panza, G. F. (1997), *Multi-scale seismicity model for seismic risk*, Bull. Seismol. Soc. Am. *87*, 1220-1229.

Montone, P., Amato, A., and Pondrelli, S. (1999), *Active stress map of Italy*, J. Geophys. Res. *104*, 25595-25610.

Mueller, B., Reinecker, J., Heidbach, O., and Fuchs, K. (2000), *The 2000 release of the World Stress Map*, http://www.world-stress-map.org.

Oldow, J. S., Ferranti, L., Lewis, D. S., Campbell, J. K., D'Argenio, B., Catalano, R., Pappone, G., Carmignani, L., Conti, P., and Aiken, C. L. V. (2002), *Active fragmentation of Adria, the north Africa promontory, central Mediterranean orogen*, Geology *30*, 779-782.

Panza, G. F., Soloviev, A. A., and Vorobieva, I. A. (1997), *Numerical modeling of block-structure dynamics: Application to the Vrancea region*, Pure Appl. Geophys. *149*, 313-336.

Panza, G. F., Pontevivo, A., Chimera, G., Raykova, R., and Aoudia, A. (2003), *The Lithosphere-Asthenosphere: Italy and surroundings*, Episodes *26*, 169-174.

Pasquale, V., Verdoya, M., Chiozzi, P., and Ranalli G. (1997), *Rheology and seismotectonic regime in the northern central Mediterranean*, Tectonophysics *270*, 239-257.

Peresan, A. and Panza, G. F. (2002), *UCI2001: The Updated Catalogue of Italy*, ICTP, Trieste, Internal report, IC/IR/2002/3.

Saraò, A., Panza, G. F., and Suhadolc, P. (1997), *Waveforms and polarities for exdended and point source studies. Earthquake fault plane solutions: data bases, derved parameters, geodynamic inferences.* In *Proceedings of the Messina University Forum on "Geodynamics of the Calabrian Arc"* (Taormina, Messina, Italy) pp. 13-17.

Scandone, P., Patacca, E., Meletti, C., Bellatalla, M., Perilli, N., and Santini, U. (1990), *Struttura geologica, evoluzione cinematica e schema sismotettonico della penisola italiana*, Atti del Convegno GNDT *1*, 119-135.

Scandone, P., Patacca, E., Meletti, C., Bellatalla, M., Perilli, N., and Santini, U. (1994), *Seismotectonic zoning of the Italian peninsula: revised version*, Working file NOV94.

Soloviev, A. A, Vorobieva, I. A., and Panza, G. F. (2000), *Modelling of block structure dynamics for the Vrancea region: Source mechanisms of the synthetic earthquakes*, Pure Appl. Geophys. *157*, 97-110.

Soloviev, A., and Ismail-Zadeh, A. (2003), *Models of dynamics of block-and-fault systems*, In *Nonlinear Dynamics of the Lithosphere and Earthquake Prediction* (eds. Keilis-Borok, V. I., and Soloviev, A. A.) (Springer-Verlag, Berlin-Heidelberg) pp. 71-139.

Venisti, N., Calcagnile, G., Pontevivo, A., and Panza, G. F. (2004), *Tomographic study of the Adriatic plate*, Pure Appl. Geophys., in press.

Vorobieva, I. A., Gorshkov, A. I., and Soloviev, A. A. (2000), *Modelling of the block structure dynamics and seismicity for the Western Alps.* In *Computational Seismology*, vol. 31 (GEOS, Moscow) pp. 154-169 (in Russian).

Ward, S. N. (1994), *Constraints on the seismotectonics of the Central Mediterranean from Very Long Baseline Interferometry*, Geophys. J. Int. *117*, 441-452.

**Table 1.1 - Experiment 1 (standard set)**

| Block | Prescribed velocities of underlying medium in cm per unit of dimensionless time | | Average transitional and angular velocities of blocks per unit of dimensionless time | | |
|---|---|---|---|---|---|
| | Vx | Vy | VX(cm) | VY(cm) | $\omega(10^{-6}$ rad) |
| I | 0 | 0 | -1.30 | -0.15 | 0.07 |
| II | 0 | 0 | -0.20 | 0.33 | -0.02 |
| III | 0 | 0 | -1.14 | 0.13 | 0.10 |
| IV | 0 | 0 | -3.33 | 4.59 | 0.26 |
| V | 0 | 0 | 1.22 | 0.58 | 0.00 |
| VI | 0 | 0 | 5.15 | 13.07 | 0.80 |
| VII | 0 | 0 | -3.40 | 2.76 | -0.12 |
| VIII | 0 | 0 | -7.56 | 9.88 | -0.04 |
| IX | 0 | 0 | -3.02 | 2.54 | -0.33 |
| X | 0 | 0 | -9.51 | 8.77 | -0.97 |
| XI | 0 | 0 | 4.03 | 2.98 | 0.46 |

| Prescribed velocities of boundary blocks in cm per unit of dimensionless time | | |
|---|---|---|
| Boundary block | Vx | Vy |
| BB1-BB3, BB6-BB9 | 0 | 0 |
| BB4 | -25.00 | 65.00 |
| BB5 | -25.00 | 65.00 |

The prescribed angle velocity $\omega = 0$ for all boundary blocks and medium underlying blocks of structure in all experiments.

**Table 1.2 - Experiment 2**

| Block | Prescribed velocities of underlying medium in cm per unit of dimensionless time | | Average transitional and angular velocities of blocks per unit of dimensionless time | | |
|---|---|---|---|---|---|
| | Vx | Vy | VX(cm) | VY(cm) | $\omega(10^{-6}$ rad) |
| I | 0 | 0 | -7.42 | 5.40 | 0.65 |
| II | 0 | 0 | 1.87 | 4.81 | -0.08 |
| III | 0 | 0 | 0.23 | 6.00 | 0.10 |
| IV | 1.20 | 45.60 | 1.70 | 38.40 | 0.42 |
| V | 33.30 | 54.60 | 20.33 | 41.19 | 1.31 |
| VI | 33.50 | 77.30 | 33.69 | 67.03 | 0.40 |
| VII | 62.70 | 65.00 | 39.19 | 15.89 | -1.05 |
| VIII | 69.60 | 74.10 | 64.31 | 68.66 | -0.05 |
| IX | 0 | 0 | 3.68 | 6.62 | 0.03 |
| X | 0 | 0 | -17.80 | 59.56 | 0.05 |
| XI | 44.40 | 63.70 | 36.04 | 56.28 | 0.99 |

| Prescribed velocities of boundary blocks in cm per unit of dimensionless time | | |
|---|---|---|
| Boundary block | Vx | Vy |
| BB1-BB3, BB6-BB9 | 0 | 0 |
| BB4 | 69.60 | 74.10 |
| BB5 | -25.00 | 65.00 |

**Table 1.3 - Experiment 4**

| Block | Prescribed velocities of underlying medium in cm per unit of dimensionless time | | Average transitional and angular velocities of blocks per unit of dimensionless time | | |
|---|---|---|---|---|---|
| | Vx | Vy | VX(cm) | VY(cm) | $\omega(10^{-6}$ rad) |
| I | 0 | 0 | -6.96 | 5.51 | 0.62 |
| II | 0 | 0 | 1.98 | 4.96 | -0.08 |
| III | 55.00 | 45.00 | 23.06 | 32.63 | -0.30 |
| IV | 1.20 | 45.60 | 5.38 | 41.73 | 0.36 |
| V | 33.30 | 54.60 | 24.58 | 41.89 | 0.98 |
| VI | 33.50 | 77.30 | 33.85 | 67.15 | 0.35 |
| VII | 62.70 | 65.00 | 38.34 | 16.28 | -1.14 |
| VIII | 69.60 | 74.10 | 64.25 | 68.69 | -0.05 |
| IX | 0 | 0 | -12.82 | 9.48 | 0.48 |
| X | 0 | 0 | -18.27 | 59.94 | 0.07 |
| XI | 44.40 | 63.70 | 37.09 | 54.84 | 1.11 |

| Prescribed velocities of boundary blocks in cm per unit of dimensionless time | | |
|---|---|---|
| Boundary block | Vx | Vy |
| BB1-BB3, BB6, BB8-BB9 | 0 | 0 |
| BB4 | 69.60 | 74.10 |
| BB5 | -25.00 | 65.00 |
| BB7 | -30.00 | 30.00 |

**Table 1.4 - Experiment 4**

| Block | Prescribed velocities of underlying medium in cm per unit of dimensionless time | | Average transitional and angular velocities of blocks per unit of dimensionless time | | |
|---|---|---|---|---|---|
| | Vx | Vy | VX(cm) | VY(cm) | $\omega(10^{-6}$ rad) |
| I | 0 | 0 | -6.49 | 5.05 | 0.58 |
| II | 0 | 0 | 1.69 | 4.46 | -0.06 |
| III | 55.00 | 45.00 | 31.92 | 36.44 | -0.56 |
| IV | 1.20 | 45.60 | 6.20 | 42.11 | 0.36 |
| V | 33.30 | 54.60 | 27.45 | 43.36 | 0.87 |
| VI | 33.50 | 77.30 | 34.03 | 67.08 | 0.36 |
| VII | 62.70 | 65.00 | 46.01 | 20.00 | -0.85 |
| VIII | 69.60 | 74.10 | 64.79 | 68.56 | -0.04 |
| IX | 0 | 0 | -12.80 | 9.48 | 0.48 |
| X | 0 | 0 | -18.29 | 59.96 | 0.07 |
| XI | 44.40 | 63.70 | 37.85 | 54.75 | 1.09 |

| Prescribed velocities of boundary blocks in cm per unit of dimensionless time | | |
|---|---|---|
| Boundary block | Vx | Vy |
| BB1-BB3, BB6, BB8-BB9 | 0 | 0 |
| BB4 | 69.60 | 74.10 |
| BB5 | -25.00 | 65.00 |
| BB7 | -30.00 | 30.00 |

**Table 1.5 - Experiment 5**

| Block | Prescribed velocities of underlying medium in cm per unit of dimensionless time | | Average transitional and angular velocities of blocks per unit of dimensionless time | | |
|---|---|---|---|---|---|
| | Vx | Vy | VX(cm) | VY(cm) | $\omega(10^{-6}$ rad) |
| I | 0 | 0 | -7.09 | 5.52 | 0.59 |
| II | 0 | 0 | 0.65 | 6.26 | -0.03 |
| III | 55.00 | 45.00 | 46.48 | 45.24 | -0.78 |
| IV | 1.20 | 45.60 | 6.68 | 43.91 | 0.33 |
| V | 33.30 | 54.60 | 35.43 | 51.60 | 0.42 |
| VI | 33.50 | 77.30 | 36.17 | 69.78 | 0.31 |
| VII | 62.70 | 65.00 | 60.80 | 24.68 | -0.08 |
| VIII | 69.60 | 74.10 | 68.66 | 70.85 | 0.00 |
| IX | 0 | 0 | 0.06 | 3.11 | 0.06 |
| X | 0 | 0 | -21.82 | 63.32 | 0.03 |
| XI | 44.40 | 63.70 | 41.13 | 58.58 | 1.02 |

| Prescribed velocities of boundary blocks in cm per unit of dimensionless time | | |
|---|---|---|
| Boundary block | Vx | Vy |
| BB1-BB3, BB6, BB8-BB9 | 0 | 0 |
| BB4 | 69.60 | 74.10 |
| BB5 | -25.00 | 65.00 |
| BB7 | -30.00 | 30.00 |

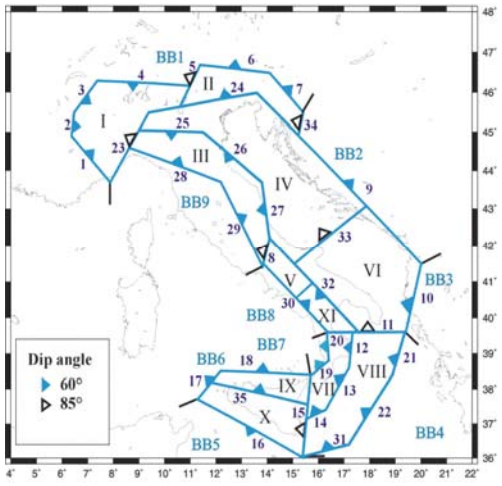


Fig. 1.1 Geometry of the block structure. I – XI – blocks; BB1- BB9 – boundary blocks.

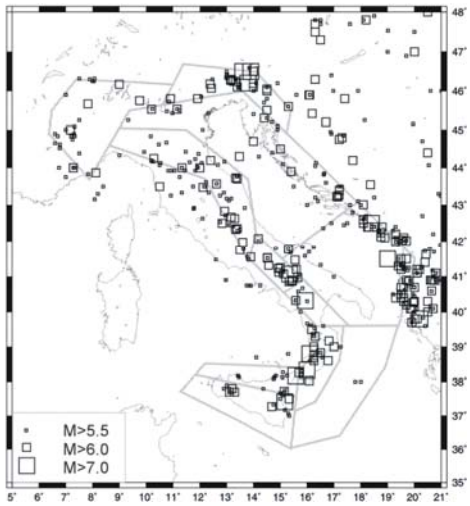


Fig. 1.2 Observed seismicity with M≥5.5, 1000-2000, (Peresan and Panza. 2002, Leydecker. 1991)

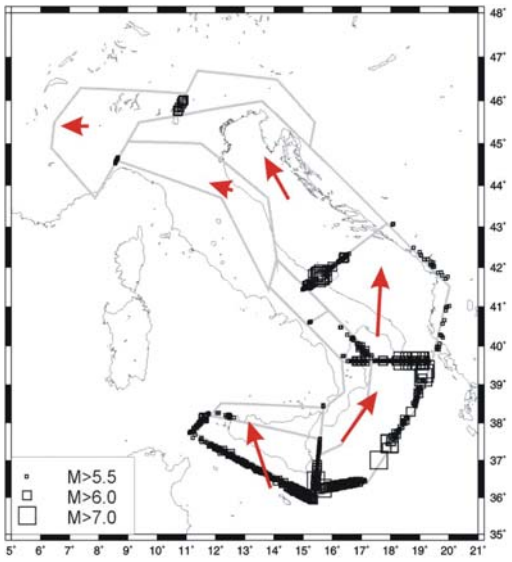


Fig. 1.3 Synthetic seismicity and movements of block structure: Experiment 1

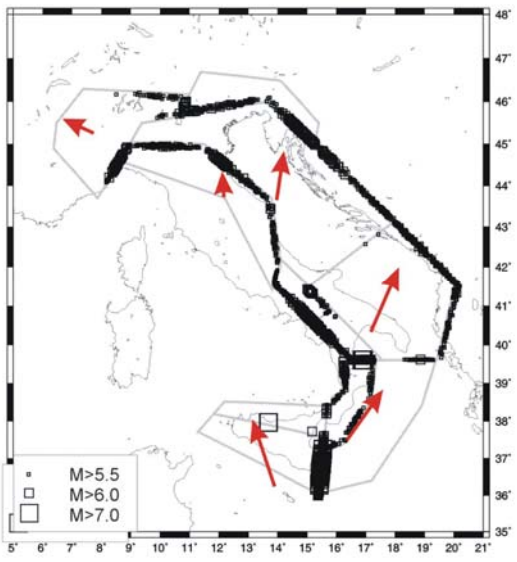


Fig. 1.4 Synthetic seismicity and movements of block structure: Experiment 2.

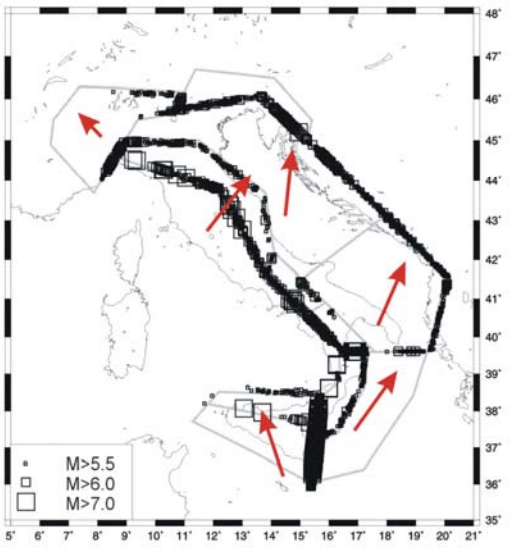


Fig. 1.5 - Synthetic seismicity and movements of block structure: Experiment 3

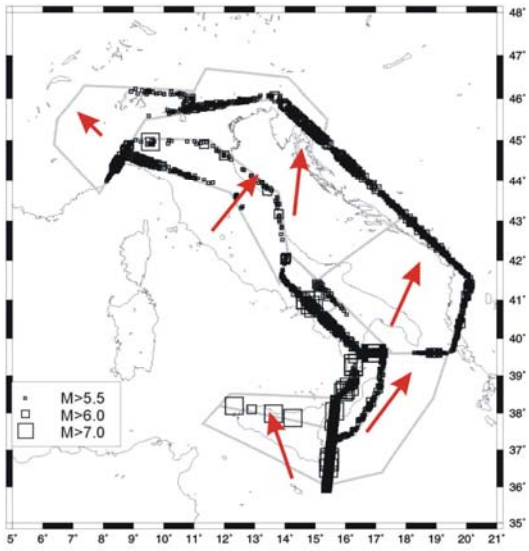


Fig. 1.6 - Synthetic seismicity and movements of block structure: Experiment 4.

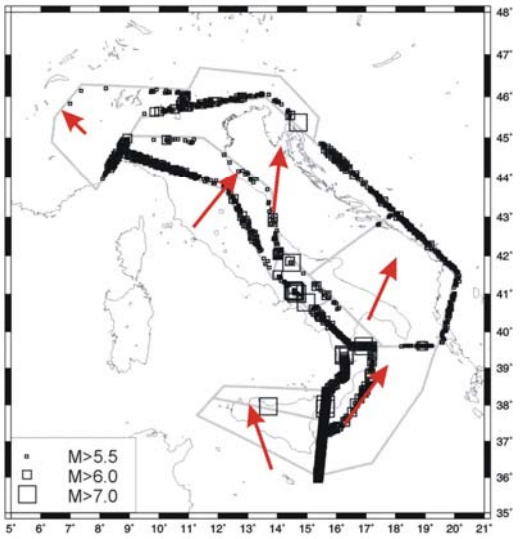


Fig. 1.7 - Synthetic seismicity and movements of block structure: Experiment 5

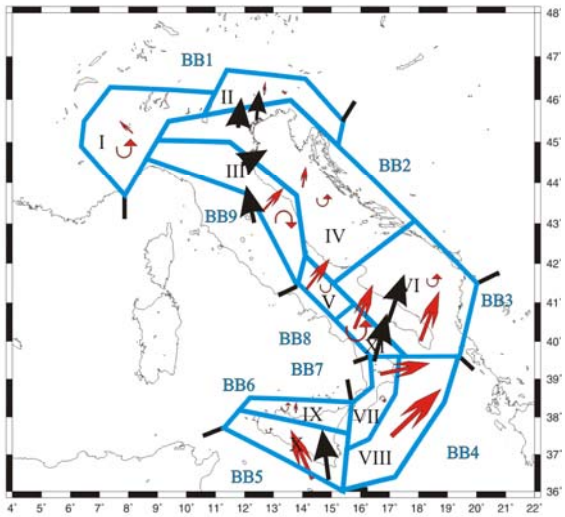


Fig. 1.8 - Comparison of the movements (open arrows) obtained in the numerical simulation of experiment 6 with the observations (fill arrows) (Devoti et al. 2002). The size of symbols is proportional to the values given in Table 1.5.

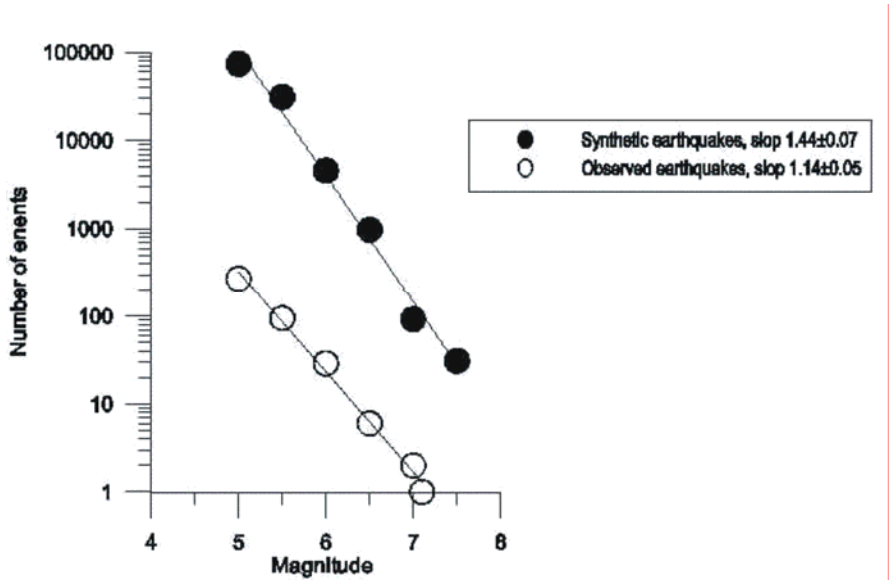


Fig. 1.9 Frequency-magnitude distribution for the synthetic (full circles) and observed (open circles) seismicity.

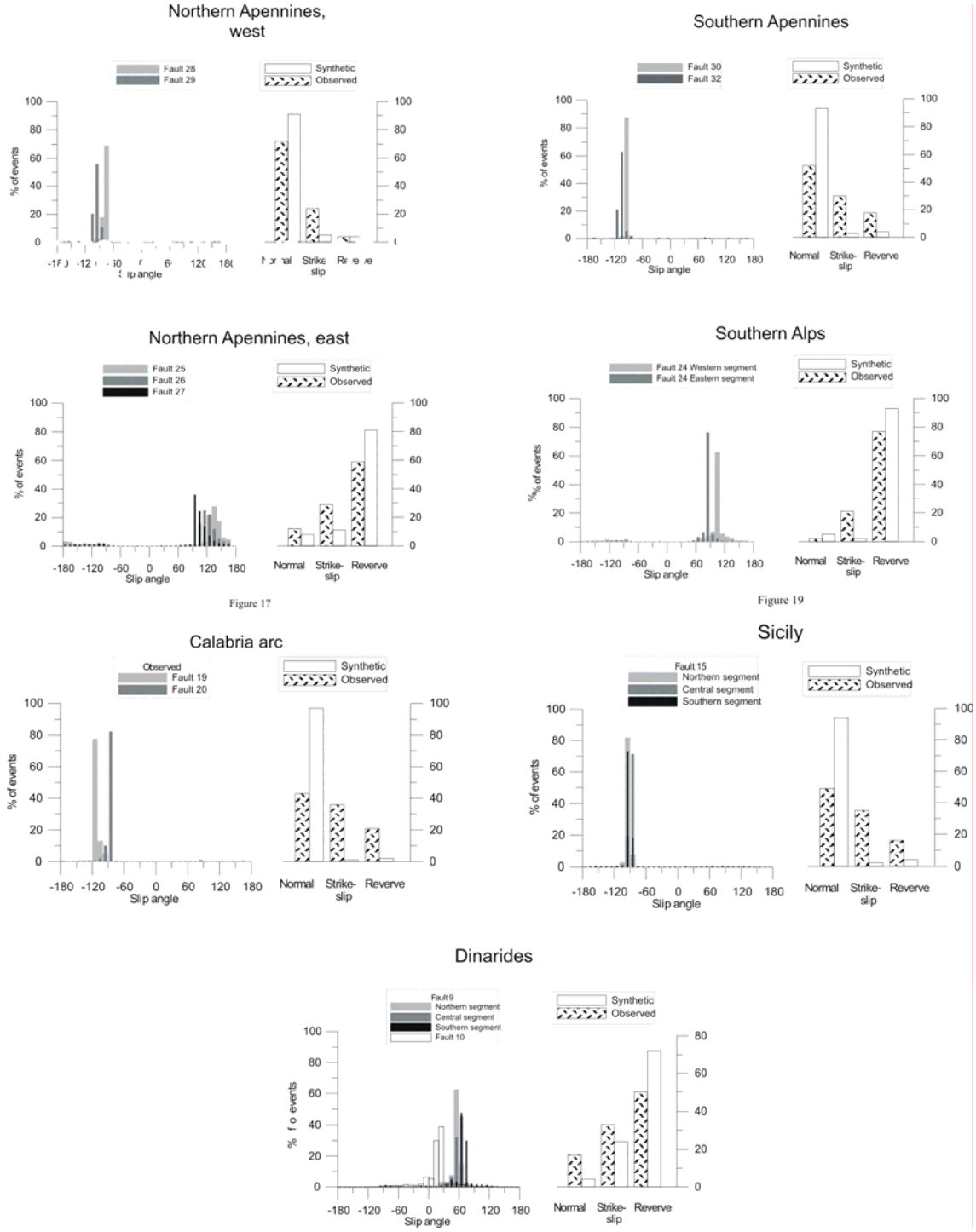


Fig. 1.10- Distribution of the slip angles for the synthetic and observed earthquakes in the different parts of tructure **1**. North-Central Apennines (faults 28, 29 in Fig. 1.1); **2**. Southern Apennines (faults 30, 32 ); **3**. North-Central Apennines (faults 25, 26 and 27 ); **4**. Southern Alps (fault 24); **5**. Calabrian Arc (faults 19, 20); **6**. Eastern edge of Sicily (fault 15); **7**. Dinarides (faults 9, 10).

# II. Block Structure Modeling of seismicity in local scale: Friuli

### 1. Block model of the Friuli region

Region Friuli is located in junction zone between eastern Alps and Dinarides. The region exhibits high seismicity: number of events with magnitude more than 6.0 (catalog UCI2006, Peresan and Panza, 2002) occurred here (Table 2.1). Such earthquakes expose seismic hazard for north-eastern Italy (Friuli-Venezia-Giulia), and, specifically, for Trieste and Udine. Figure 2.1 displays the recorded seismicity in the region starting from magnitude 4.0 (Peresan and Panza, 2002).

*Table 2.1.* Large earthquakes in the vicinity of Eastern Alps and Didarides junction, UCI2006.

| Date | | | epicenter | | | |
|---|---|---|---|---|---|---|
| yyyy | mm | dd | lat | lon | dep | *M* |
| 1873 | 6 | 29 | 46.15 | 12.38 | 25 | 6.33 |
| 1936 | 10 | 18 | 46.05 | 12.42 | 18 | 6.20 |
| 1963 | 5 | 19 | 46.1 | 14.8 | 13 | 6.00 |
| 1976 | 5 | 6 | 46.23 | 13.13 | 12 | 6.52 |
| 1976 | 6 | 17 | 46.08 | 12.93 | 14 | 6.10 |
| 1976 | 6 | 17 | 46.45 | 13.5 | 35 | 6.10 |
| 1976 | 9 | 15 | 46.3 | 13.18 | 2 | 6.00 |
| 1976 | 9 | 15 | 46.25 | 13.13 | 12 | 6.00 |
| 1998 | 4 | 12 | 46.24 | 13.65 | 10 | 6.00 |

There are additional data for this territory that have information about other significant earthquakes. Earthquakes with magnitude more than 6.0 from global catalog NEIC are presented in Table 2.2, from Earthquake catalog for Central and Southeastern Europe (Shebalin et al., 1998) in Table 2.3.

*Table 2.2.* Large earthquakes in the vicinity of Eastern Alps and Didarides junction, NEIC.

| Date | | | epicenter | | | |
|---|---|---|---|---|---|---|
| yyyy | mm | dd | lat | lon | dep | *M* |
| 1511 | 3 | 26 | 46.1 | 14 | 7 | 6.90 |
| 1695 | 2 | 25 | 45.4 | 12.2 | 0 | 6.20 |
| 1695 | 2 | 25 | 45.4 | 12.2 | 0 | 6.20 |
| 1895 | 4 | 14 | 46.1 | 14.5 | 16 | 6.10 |
| 1895 | 4 | 1 | 46.1 | 14.5 | 16 | 6.10 |
| 1963 | 5 | 19 | 46 | 14.6 | 32 | 6.00 |
| 1976 | 5 | 6 | 46.35 | 13.27 | 9 | 6.50 |
| 1976 | 6 | 17 | 46.16 | 12.86 | 24 | 6.10 |
| 1976 | 9 | 15 | 46.3 | 13.19 | 10 | 6.00 |
| 1998 | 4 | 12 | 46.25 | 13.65 | 10 | 6.00 |

*Table 2.3.* Large earthquakes in the vicinity of Eastern Alps and Didarides junction, Shebalin et al., 1998.

| Date | | | epicenter | | | |
|---|---|---|---|---|---|---|
| yyyy | mm | dd | lat | lon | dep | *M* |
| 792 | 2 | 1 | 46 | 14.5 | 16 | 6.0 |
| 1000 | 3 | 29 | 46.5 | 14 | 28 | 6.9 |
| 1348 | 1 | 25 | 46.5 | 13.6 | 26 | 7.9 |
| 1511 | 3 | 26 | 46.2 | 13.8 | 20 | 7.4 |
| 1511 | 8 | 8 | 46.1 | 13.4 | 10 | 6.3 |
| 1551 | 3 | 26 | 46.2 | 14 | 22 | 6.3 |
| 1690 | 12 | 4 | 46.5 | 13.9 | 28 | 7.5 |
| 1721 | 1 | 12 | 45.3 | 14.4 | 10 | 6.1 |
| 1870 | 3 | 1 | 45.5 | 14.5 | 16 | 6.4 |
| 1895 | 4 | 14 | 46.05 | 14.5 | 17 | 6.1 |

The last catalog (Shebalin et al., 1998) presents information about a number of historical large events with magnitude more than 7.0, in particularly, the 1348 ($M$=7.9) and 1690 ($M$=7.5) earthquakes, that sit near the Fella-Sava and Insubric lines, but their location and magnitudes are disputable. Probably they have lesser magnitudes and are connected with Periadriatic overthrust, as accuracy of the epicenter determination is poor for historical events.

The study region includes the Adria plate in the south, Eastern Alps in the north and Dinarides in the east. The most seismically active faults are Periadriatic overthrust, Idrija line near Periadriatic line, and Adria boundary east to the Istria peninsula. (Figure 2.1).

To outline the fault-and-block geometry, we use the morphostructural zoning maps of the Alps and Dinarides (Gorshkov et al., 2004) as well as spatial pattern of the recorded seismicity. The map of lineaments as well as seismicity with magnitude more than 4.0 is shown in the Figure 2.1. The major structural boundary between the Alps and the Dinarides is given by the first rank (lineament I in Figure 2.1). It is traced along the latitude of the town of Tolmin, where, according to CAROBENE & CARULLI (1981) and CARULLI *et al.* (1990), the major tectonic orientation changes from Alpine to Dinaric. It is continued to the west by Periadriatic overthrust (lineament II in Figure 2.1) that separates Adria plate from the Southern Alps. The location of this boundary is also in agreement with other studies (PRELOGOVIĆ *et al.* 1998; POLJAK *et al.* 2001). The lineament of second rank corresponds to the Insubric-Giudicarie-Periadriatic (line III in Figure 2.1), which is a fault crosscutting a large part of the Alps (DOGLIONI, 2000). The lineament IV in Figure 2.1, that divides the Venetian Southern Alps into two megablocks, corresponds to a sinistral strike-slip zone (MELETTI *et al.* 2000). The western and eastern limits of the Dinarides, the first rank lineaments V and VI in Figure 2.1, separate the Dinarides from the Adriatic marine basin and Pannonian basin. Seismically active Idrija line is represented by the third rank lineament VII (Figure 2.1). The transverse second rank E-W lineament VIII (Figure 2.1) intersects Dinadides and separates more elevated areas to the south, from lower areas to the north. The lineament is traced along rectilinear segments of river valleys flowing in E-W direction. The second rank lineament IX (Figure 2.1) is traced along the Adriatic coast.

The comparison of the morphostructural map with the recorded seismicity shows that large clusters of seismicity correlate with lineaments shown in Figure 2.1, therefore we can use morphostructural map (Figure 2.1) to model seismicity in the Friuli region.

The block structure consists of six blocks (Figure 2.2) that are outlined by 16 faults. Faults are traced along the lineaments of morphostructural zoning. The SW boundary of the structure corresponds to the first rank lineaments II and V, which separate the Alps and Dinarides from the Adria plate and second rank lineament IX that corresponds to the Adriatic coast. Northern boundary of the structure is the Insubric line (second rank lineament III), while the western boundary is lineament IV. Eastern boundary is traced along the lineament VI separating the Dinarides and Pannonian basin.

Two blocks in the north (B1 and B2-4 in Figure 2.2) represent the Southern Alps. Alps and Dinarides are separated by the first rank lineaments I and II (the Periadriatic overthrust). Four southern blocks (B3-B6 in Figure 2.3) represent the Dinarides. Transversal second rank lineament intersects Dinarides in E-W direction and separates two northern blocks from two southern ones. The Idrija line (lineament of the third rank) divides the structure into western and eastern parts.

Eight boundary blocks are introduced to prescribe external forces acting in the region. Boundary blocks BB1 and BB2 delimit structure from the west and north respectively. Boundary block BB3 is eastern edge of Dinarides, BB6 is southern boundary of structure. BB5-BB8 represents the boundary of Adria plate.

To define thickness of the block structure the information about distribution of seismicity in the depth (Figure 2.3) is used. Most part of events have depth within 20km, but seismisity extends to 40km. Another data are structural model of Italy (Chimera e. al.). (Figure 2.4). Two structural boundaries could be distinguished: the first one is Moho in the depth about 40 km that is in agreement with European Moho map (Cloetingh et al., 2006). Another structural boundary

has depth about 20km. Thus the available information allows choose the thickness of layer 40km or 20km, and both variatns will be studied.

The proper choice of the dip angles of the faults is essential for the quality of modeling of seismicity. In correspondence with seismotectonic model of Garulli et al. (1990), the Idrija line and Insubric line are subvertical faults, while the Periadriatic overthrust is inclined fault. To define dip angles more precisely the information about fault plane solutions (FPS) is used. The Friuli earthquake of 1976 occurred in the Periadriatic overthrust (fault 10 of the block structure), its FPS shows reverse faulting mechanism and dip angle about 30 degrees (Aoudia et al., 2000). Another large earthquake Bovec 1998 occurred to the east from Friuli 1976, where Idrija line (Fault 14 of the structure) intersects the boundary between Alps and Dinarides. It had right lateral strike-slip mechanism and subvertical dip angle (Bajc et al., 2001). To estimate dip angles for the whole structure the FPS from DST Data Base in the territory under study are associated with the faults of block structure. The average dip angles are given for each fault. The data are most reliable for Periadriatic line (faults 10, 11, 16), Idria line (fault 14) and western boundary of structure (fault 1). There are no FPS data for some faults. The following values of dip angles were chosen (Table 2.4)

*Table 2.4.*Average dip anles from FPS and in the block structure.

| Fault | Dip angle | | Fault | Dip angle | | Fault | Dip angle | | Fault | Dip angle | |
|---|---|---|---|---|---|---|---|---|---|---|---|
| | Observed | Structure | | Observed | Structure | | Observed | Structure | | Observed | Structure |
| 1 | 88.3 | 88 | 5 | - | 80 | 9 | 62.0 | 70 | 13 | 90.0 | 85 |
| 2 | 82.1 | 80 | 6 | - | 60 | 10 | 33.5 | 35 | 14 | 75.5 | 75 |
| 3 | 63.0 | 70 | 7 | - | 80 | 11 | - | 35 | 15 | - | 80 |
| 4 | - | 70 | 8 | - | 80 | 12 | 46.5 | 45 | 16 | 49.8 | 45 |

The visco-elastic features are the same for all the faults and block bottoms: elastic coefficient $K$=1.0, coefficients controlling viscosity $W$=0.05, $Ws$ = 50.00, the ratio of shear to normal stress, controlling earthquake occurrence in the model $B$ =0.10, $Hf$ = 0.085, $Hs$ = 0.07. The size of the sell ε=2km that allows model seismicity from magnitude 4.

The movement of the Adria is supposed to be the basic factor controlling geodynamics and seismicity in the studied region. All external driving forces are prescribed in southern boundary of the structure along the Adria plate. To choose the direction and relative values we used the results of the block structure modeling for the whole Italy and its surroundings (Peresan et al, in press); the GPS observations (D'Agostino et al., 2005). In the first case we prescribe the velocity of Adria plate generally in the north direction, as it was obtained for the Northern part of Adria (Peresan et al, In press). The value and direction slightly vary along the boundary due to the rotation of Adria. They are given in the left columns of Table 2.5. The GPS observations are shown in the Figure 2.5 (after D'Agostino et al., 2005). The movement of Adria has some western component, authors estimate azimuth as -10$^o$ in the vicinity of Trieste. The value of velocity decreases to the west of region and change direction to the north. As we use dimensionless time while modeling, only directions and relative values were taken into account. The absolute values were chosen to be approximately the same, as in modeling in the regional scale. The velocities of boundary blocks for second variant are given in the right columns of Table 2.5.

*Table 2.5.* Prescribed velocities of boundary blocks in *cm* per unit of dimensionless time

| Boundary Block | Velocities obtained from whole Italy modeling (Peresan et al., in press) | | Velocities from GPS observations (D'Agostino et al., 2005) | |
|---|---|---|---|---|
| | ***Vx* (East)** | ***Vy* (North)** | ***Vx* (East)** | ***Vy* (North)** |
| 1 | 0.0 | 0.0 | 0.0 | 0.0 |
| 2 | 0.0 | 0.0 | 0.0 | 0.0 |
| 3 | 0.0 | 0.0 | 0.0 | 0.0 |
| 4 | 1.0 | 22.0 | -4.0 | 22.0 |
| 5 | 2.0 | 44.0 | -8.0 | 45.0 |
| 6 | 1.0 | 45.0 | -8.0 | 45.0 |
| 7 | 0.0 | 46.0 | -8.0 | 45.0 |
| 8 | -1.0 | 48.0 | 0.0 | 30.0 |

**Results of modeling**

Four variants are presented: first two variants are for the prescribed velocities of Adria obtained from the modeling in the regional scale (Reresan et al., in press), two others are for velocities prescribed in accordance with GPS observations (D'Agostino et al., 2005). All variants were obtained for 100 units of dimensionless time.

The movements of the blocks of the structure are given in Tables 2.6, 2.7

*Table 2.6* Velocities of blocks obtained for prescribed velocities of boundary from Peresan et al. (in press). Values are given in *cm* for transition and in $rad \cdot 10^{-5}$ for rotation per unit of dimensionless time

| Block | Depth 40km | | | Depth 20km | | |
|---|---|---|---|---|---|---|
| | *Vx* | *Vy* | ω | *Vx* | *Vy* | ω |
| 1 | 0.05 | 1.21 | 0.017 | 0.06 | 1.17 | 0.015 |
| 2 | -0.006 | 0.97 | 0.185 | -0.08 | 1.05 | 0.179 |
| 3 | 4.43 | 17.83 | 0.186 | 2.41 | 12.08 | 0.579 |
| 4 | 6.92 | 19.01 | 0.108 | 5.89 | 15.44 | 0.662 |
| 5 | 5.74 | 26.75 | -0.212 | 5.84 | 16.17 | -0.202 |
| 6 | 4.92 | 26/66 | -0.047 | 5.22 | 16.18 | -0.061 |

*Table 2.7* Velocities of blocks obtained for prescribed velocities of boundary from D'Agostino et al. (2005). Values are given in *cm* for transition and in $rad \cdot 10^{-5}$ for rotation per unit of dimensionless time

| Block | Depth 40km | | | Depth 20km | | |
|---|---|---|---|---|---|---|
| | *Vx* | *Vy* | ω | *Vx* | *Vy* | ω |
| 1 | 0.05 | 1.15 | 0.016 | 0.06 | 1.17 | 0.015 |
| 2 | -0.30 | 1.04 | 0.184 | -0.17 | 1.05 | 0.171 |
| 3 | 0.78 | 17.46 | 0.101 | 0.86 | 11.05 | 0.336 |
| 4 | 0.11 | 18.68 | 0.152 | 1.42 | 13.47 | 0.473 |
| 5 | -0.82 | 24.28 | -0.101 | 1.40 | 14.74 | -0.162 |
| 6 | 0.02 | 23.73 | 0.026 | 1.99 | 14.48 | -0.012 |

For the all variants blocks 1 and 2 representing Alps moves very slowly. Four blocks (B3-B6) representing Dinarides move much faster. The general direction of movement is North, with some East component in the case of movements from Peresan et al. (in press). The western blocks (B5, B6) move faster than eastern ones (B3, B4). Velocities are commonly higher for the thickness of layer 40km, than for 20km.

The frequency of occurrence graphs (Gutenberg-Richter plots) are given in the Figure 2.6. The observed relation for the depth 20 and 40 are presented in the same Figure 2.6. They are constructed by UCI2006 catalog for the period 1870-2006, when catalog is representative for magnitude 4.0. The plots for synthetic seicmicity are pretty good linear for the thickness of layer 40km, the linearity is partly lost for 20 km: there is lack of the intermediate magnitude events in the range 5 ÷ 6; nevertheless, the shape of plots for thickness 20km has some similarity with the shape of the observed one. The best fit linear relations for observed and synthetic seismicity are:

| | | | |
|---|---|---|---|
| $\lg(N) = -0.955\,M + 6.426;$ | $\sigma = 0.113$ | Observed $H$=40km | (1) |
| $\lg(N) = -0.953\,M + 6.270;$ | $\sigma = 0.108$ | Observed $H$=20km | (2) |
| $\lg(N) = -0.963\,M + 8.710;$ | $\sigma = 0.055$ | Pesesan, $H$=40km | (3) |
| $\lg(N) = -0.922\,M + 8.168;$ | $\sigma = 0.122$ | Pesesan, $H$=20km | (4) |
| $\lg(N) = -0.955\,M + 8.526;$ | $\sigma = 0.058$ | D'Agostino $H$=40km | (5) |
| $\lg(N) = -0.920\,M + 7.986;$ | $\sigma = 0.166$ | D'Agostino $H$=20km | (6) |

The slope of linear relation is the same for observed and synthetic seismicity for the depth 40km. It allows estimate the duration of the unit of dimensionless time. The duration of observations is 135 years; the duration of simulation is 100 units. Then, from (1), (3) and (5) the duration of one unit $\tau$ is approximately 200years. The estimation for 20 km from (2), (4) and (6) gives the value of $\tau$ 100years. Than the velocity of Adria is 2.5÷4.5 mm/ per year. The obtained value is in accordance with the observations (i.e. D'Agostiono et al., 2005, Jimenez-Munt et al., 2003, Nocquet et al., 2003,)

The spatial distribution of synthetic seismicity for four variants of modeling is presented in the Figures 2.7, 2.8. The maximum magnitude of the synthetic events exceeds 7.0, it is 7.3 for the thickness of layer 40 km. and 7.1 for 20km. These values are larger than maximum observed magnitude 6.5 given in UCI2006 catalog (Table 2.1). Nevertheless, NEIC reports maximum magnitude 6.9 (1511), and the equivalent magnitude of the Friuli series (1976) is estimated more than 7. These facts confirm that the structure is powerful to generate earthquake with magnitude 7 or more, in spite of the absence of reliable recorded data.

The distribution of epicenters is very similar for different prescribed velocities, but it changes with the change of depth. Level of activity considerably decreases, and seismicity does not penetrate to the eastern part of the structure with decreasing of the thickness of layer. The largest synthetic events occur in the Periadriatic overthrust for the all variants of modeling, another cluster of large synthetic events is connected with Adriatic coast to the east of Istria. The boundary between the Alps and Dinarides that exhibits highest level of observed seismicity in the studied region is active in the model when thickness of layer is 40km. High level of seismic activity obtained for eastern boundary of Dinarides in case of thickness 40. Observations do not exhibit high level of activity here, but earthquakes of magnitude more than 6 occurred here. In correspondence with the results of recognition of seismogenic nodes in the Alps and Dinarides (Gorshkov et al., 2004), almost the entire territory under study is prone to earthquakes with magnitude $M \geq 6.5$ (Figure 2.9). So, the result of modeling does not contradict to the available information.

The detailed information about number of events, maximum magnitude, and focal mechanisms of synthetic events that occur in the different faults of the structure is given in the Tables 2.8-2.11 for the all variants of modeling. Earthquakes do not occur in the northern part of the structure in all variants. This territory does no exhibit the considerable level of the observed seismic activity also. The set of faults and segments where synthetic earthquakes occur is almost the same in the different variants. Maximum magnitudes ale similar for different prescribed movements, but differ with the changing of the thickness of layer.

The FPS for synthetic events are: reverse faulting for Periadriatic line (faults 10, 11) and boundary between Alps and Dinarides (faults 12, 16), they have some left-lateral strike-slip component in the western part of Periadriatic (fault 11).. Adriatic coast (faults 6-9), Idrja line (fault14) and Easter boundary of the structure (faults 3-4) shows reverse faulting with considerable right-lateral strike-slip component. That is in correspondence with the available observations (Tables 2.12, 2.13).

*Table 2.8.* Synthetic seismicity obtained for prescribed velocities of boundary from Peresan et al. (in Press), depth of layer 40km

| Segment* | Fault | Left block | Right block | Number of events | Maximum magnitude | Slip angle |
|---|---|---|---|---|---|---|
| 1 | 1 | bb1 | b1 | 94 | 5.05 | -70 |
| 5 | 3 | bb3 | b3 | 7333 | 6.8 | 110 |
| 6 | 4 | bb3 | b3 | 6151 | 6.95 | 110 |
| 7 | 4 | bb3 | b4 | 10730 | 7.15 | 110 |
| 9 | 7 | b5 | bb5 | 47 | 7.0 | 110 |
| 10 | 8 | b5 | bb6 | 118 | 6.8 | 135 |
| 11 | 8 | b6 | bb6 | 125 | 7.0 | 135 |
| 12 | 9 | b6 | bb7 | 1564 | 7.2 | 140 |

| | | | | | | |
|---|---|---|---|---|---|---|
| 13 | 9 | b1 | bb8 | 5108 | 5.85 | 180 |
| 14 | 10 | b1 | bb8 | 1423 | 6.75 | 100 |
| 15 | 11 | b1 | bb8 | 935 | 7.25 | 75 |
| 16 | 15 | b4 | bb5 | 2655 | 6.65 | 150 |
| 18 | 15 | b3 | b6 | 30 | 6.1 | 140 |
| 19 | 6 | b5 | bb5 | 261 | 6.95 | 120 |
| 20 | 12 | b2 | b3 | 2463 | 7.35 | 90 |
| 23 | 14 | b3 | b6 | 1247 | 7.25 | 125 |
| 24 | 14 | b2 | b6 | 4868 | 6.4 | 115 |
| 26 | 16 | b1 | b6 | 2327 | 7.25 | 90 |

* Only the segments where synthetic events occurred are presented

*Table 2.9* Synthetic seismicity obtained for prescribed velocities of boundary from Peresan et al. (in Press), depth of layer 20km

| Segment* | Fault | Left block | Right block | Number of events | Maximum magnitude | Slip angle |
|---|---|---|---|---|---|---|
| 5 | 3 | bb3 | b3 | 2634 | 5.9 | 110 |
| 6 | 4 | bb3 | b3 | 4203 | 6.3 | 120 |
| 7 | 4 | bb3 | b4 | 7424 | 7.1 | 110 |
| 8 | 5 | b4 | bb4 | 642 | 5.8 | 110 |
| 9 | 7 | b5 | bb5 | 140 | 6.55 | 100 |
| 10 | 8 | b5 | bb6 | 107 | 6.6 | 130 |
| 11 | 8 | b6 | bb6 | 74 | 6.65 | 130 |
| 12 | 9 | b6 | bb7 | 910 | 6.9 | 125 |
| 13 | 9 | b1 | bb8 | 897 | 5.95 | 120 |
| 14 | 10 | b1 | bb8 | 528 | 6.75 | 100 |
| 15 | 11 | b1 | bb8 | 509 | 7.05 | 75 |
| 16 | 15 | b4 | bb5 | 2720 | 6.5 | 145 |
| 17 | 15 | b4 | b5 | 79 | 4.9 | -95 |
| 19 | 6 | b5 | bb5 | 918 | 6.8 | 125 |
| 20 | 12 | b2 | b3 | 1259 | 5.25 | 95 |
| 23 | 14 | b3 | b6 | 1026 | 5.8 | 115 |
| 24 | 14 | b2 | b6 | 1720 | 5.8 | 115 |
| 26 | 16 | b1 | b6 | 419 | 6.95 | 90 |

* Only the segments where synthetic events occurred are presented

*Table 2.10* Synthetic seismicity obtained for prescribed velocities of boundary from D'Agostino et al. (2005), depth of layer 40km

| Segment | Fault | Left block | Right block | Number of events | Maximum magnitude | Slip angle |
|---|---|---|---|---|---|---|
| 1 | 1 | bb1 | b1 | 25 | 4.45 | -60 |
| 5 | 3 | bb3 | b3 | 5877 | 6.85 | 115 |
| 6 | 4 | bb3 | b3 | 3106 | 7.25 | 140 |
| 7 | 4 | bb3 | b4 | 5106 | 7.2 | 135 |
| 9 | 7 | b5 | bb5 | 66 | 7.0 | 105 |
| 10 | 8 | b5 | bb6 | 33 | 6.9 | 145 |
| 11 | 8 | b6 | bb6 | 624 | 6.85 | 155 |
| 12 | 9 | b6 | bb7 | 1194 | 7.2 | 135 |
| 13 | 9 | b1 | bb8 | 1903 | 6.25 | 115 |
| 14 | 10 | b1 | bb8 | 965 | 6.75 | 100 |
| 15 | 11 | b1 | bb8 | 553 | 7.25 | 75 |
| 16 | 15 | b4 | bb5 | 7103 | 6.9 | 180 |
| 19 | 6 | b5 | bb5 | 411 | 6.95 | 135 |
| 20 | 12 | b2 | b3 | 3826 | 7.35 | 95 |
| 23 | 14 | b3 | b6 | 913 | 7.0 | 140 |
| 24 | 14 | b2 | b6 | 3489 | 6.55 | 115 |
| 26 | 16 | b1 | b6 | 2581 | 7.1 | 95 |

* Only the segments where synthetic events occurred are presented

*Table 2.11* Synthetic seismicity obtained for prescribed velocities of boundary from D'Agostino et al. (2005), depth of layer 20km

| Segment* | Fault | Left block | Right block | Number of events | Maximum magnitude | Slip angle |
|---|---|---|---|---|---|---|
| 5 | 3 | bb3 | b3 | 1953 | 6.45 | 115 |
| 6 | 4 | bb3 | b3 | 2617 | 6.95 | 125 |
| 7 | 4 | bb3 | b4 | 5907 | 5.65 | 130 |
| 8 | 5 | b4 | bb4 | 715 | 6.25 | 115 |
| 9 | 7 | b5 | bb5 | 70 | 6.55 | 110 |
| 10 | 8 | b5 | bb6 | 119 | 6.55 | 140 |
| 11 | 8 | b6 | bb6 | 256 | 6.65 | 145 |
| 12 | 9 | b6 | bb7 | 391 | 7.0 | 130 |
| 13 | 9 | b1 | bb8 | 617 | 5.90 | 115 |
| 14 | 10 | b1 | bb8 | 331 | 6.75 | 105 |
| 15 | 11 | b1 | bb8 | 226 | 7.05 | 75 |
| 16 | 15 | b4 | bb5 | 4718 | 5.55 | 180 |
| 17 | 15 | b4 | b5 | 6 | 4.75 | 135 |
| 19 | 6 | b5 | bb5 | 5418 | 6.8 | 135 |
| 20 | 12 | b2 | b3 | 8259 | 5.6 | 105 |
| 23 | 14 | b3 | b6 | 150 | 5.658 | 115 |
| 24 | 14 | b2 | b6 | 9080 | 6.258 | 115 |
| 26 | 16 | b1 | b6 | 106 | 6.95 | 90 |

* Only the segments where synthetic events occurred are presented

*Table 2.12*. Comparision of the observed and synthetic FPS, for prescribed velocities of boundary from Peresan et al. (in Press)

| Fault | slip angle Obs., 40km, 20km | | | Fault | slip angle Obs., 40km, 20km | | | Fault | slip angle Obs., 40km, 20km | | | Fault | slip angle Obs., 40km, 20km | | |
|---|---|---|---|---|---|---|---|---|---|---|---|---|---|---|---|
| 1 | -3.5 | -70 | - | 5 | - | 110 | - | 9 | 142 | 140 | 125 | 13 | 96 | - | - |
| 2 | -179 | - | - | 6 | - | 125 | 120 | 10 | 84 | 100 | 100 | 14 | 130 | 125 | 115 |
| 3 | 100 | 110 | 110 | 7 | - | 110 | 100 | 11 | 54 | 75 | 75 | 15 | - | 140 | 145 |
| 4 | - | 110 | 110 | 8 | - | 135 | 130 | 12 | - | 90 | - | 16 | 49.8 | 90 | 90 |

*Table 2.13*. Comparision of the observed and synthetic FPS, for prescribed velocities of boundary from D'Agostino et al. (2005)

| Fault | slip angle Obs., 40km, 20km | | | Fault | slip angle Obs., 40km, 20km | | | Fault | slip angle Obs., 40km, 20km | | | Fault | slip angle Obs., 40km, 20km | | |
|---|---|---|---|---|---|---|---|---|---|---|---|---|---|---|---|
| 1 | -3.5 | -60 | - | 5 | - | - | 115 | 9 | 142 | 130 | 125 | 13 | 96 | - | - |
| 2 | -179 | - | - | 6 | - | 135 | 135 | 10 | 84 | 100 | 105 | 14 | 130 | 115 | 115 |
| 3 | 100 | 115 | 115 | 7 | - | 105 | 110 | 11 | 54 | 75 | 75 | 15 | - | 180 | 145 |
| 4 | - | 135 | 125 | 8 | - | 145 | 140 | 12 | - | 95 | 105 | 16 | 49.8 | 90 | 90 |

The results of modeling show that detailed analysis of the available observations and the results of modeling in the regional scale allows to model seismisity in the local scale more realistic. The thickness of layer 40 km is preferable, it provides the features of synthetic seismicity closer to observations. The results are similar for both variants of the prescribed velocities as the directions are close each to other. The geometry of block structure including proper choice of the dip angles and thickness of the structure is more important for the successful modeling.

# References


A. AOUDIA, A. SARAO, B. BUKCHIN, AND P. SUHADOLC (2000*) The 1976 Friuli (NE Italy) Thrust Faulting Earthquake: A Reappraisal 23 Years Later*. Geophysical Research Letters, VOL. 27, NO. 4, PAGES 573-576, 2000

J. BAJC, A. AOUDIA, A. SARAO, AND P. SUHADOLC (2001). *The 1998 Bovec-Krn mountain (Slovenia) earthquake sequence.* Geophysical Research Letters, VOL. 28, NO. 9, PAGES 1839-1842, 2001

CARULLI G.B., NICOLICH R., REBEZ A. & SLEJKO D. (1990) - Seismotectonics of the Northwest External Dinarides. *Tectonophysics*, **179**, 11-25.

CHIMERA, G., AOUDIA, A., SARAÒ, A., AND PANZA, G. F. (2003), *Actives tectonics in Central Italy: constraints from surface wave tomography and source moment tensor inversion*, Phys. Earth Planet. Inter. *138*, 241-262.

N. D'AGOSTINO, D. CHELONI, S. MANTENUTO, G. SELVAGGI, A. MICHELINI, AND D. ZULIANI. (2005) *Strain accumulation in the southern Alps (NE Italy) and deformation at the northeastern boundary of Adria observed by CGPS measurements.* Geophysical Research Letters, VOL. 32, L19306, doi:10.1029/2005GL024266, 2005

S. CLOETINGH, T.TORNU, P.A.ZIEDLER, F.BEEKMAN.(2006) *Neotectonics and intrapalte topography of the northern Alpine Foreland.* Earth-science Reviews 74) p127-196, 2006

DOGLIONI C. (2000) - *Sismotettonica dell'Italia nord-orientale e possibile comparazione con gli Appennini.* In: GALADINI F., MELETTI C. & REBEZ A. (Eds), Le ricerche del GNDT nel campo della pericolosità sismica (1996-1999), CNR-Gruppo Nazionale Difesa Terremoti, Roma, 51-58.

FPS DST data file (2006)

GORSHKOV A.I., PANZA G.F., SOLOVIEV A.A., AOUDIA A. (2004). *Identification of seismogenic nodes in the Alps and Dinarides* Bolletino della Societa Geologica Italiana, **123**, 3-18.

JIMENEZ-MUNT, I., SABADINI, R., AND GARDI, A. (2003), *Active deformation in the Mediterranean from Gibraltar to Anatolia inferred from numerical modeling and geodetic and seismological data*, J. Geophys. Res. *108* (B1), 1-24.

MELETTI C., PATACCA E. & SCANDONE P. (2000) - *Construction of a seismotectonic model: the case of Italy*. Pure Appl. Geophys., **157**, 11-35.

NEIC *Hypocenter data file*. http://neic.usgs.gov

NOCQUET, J. M., AND CALAIS, E. (2003), *Crustal velocity field of western Europe from permanent GPS array solutions, 1996–2001*, Geophys. J. Int. *154*, 72–88.

PERESAN, A. AND PANZA, G. F. (2002), *UCI2006: The Updated Catalogue of Italy*, ICTP, Trieste, Internal report, IC/IR/2002/3.

A. PERESAN, I. VOROBIEVA, A. SOLOVIEV, G.F. PANZA. *Block structure modeling of seismicity in the Italian Area and surroundings* . Pageoph, in press

PRELOGOVIĆ E., SAFTIĆ B., KUK V., VELIĆ J., DRAGAŠ M. & LUČIĆ D. (1998) - *Tectonic activity in the Croatian part of the Pannonian basin.* Tectonophysics, **298**, 283-293.

SHEBALIN N., LEYDECKER G., MOKRUSHINA N., TATEVOSIAN R., ERTELEVA M. & VASSILIEV V. (1998) - *Earthquake catalogue for Central and Southeastern Europe 342 BC - 1990 AD.* European Commission, Report No. ETNU CT 93-0087, Brussels.

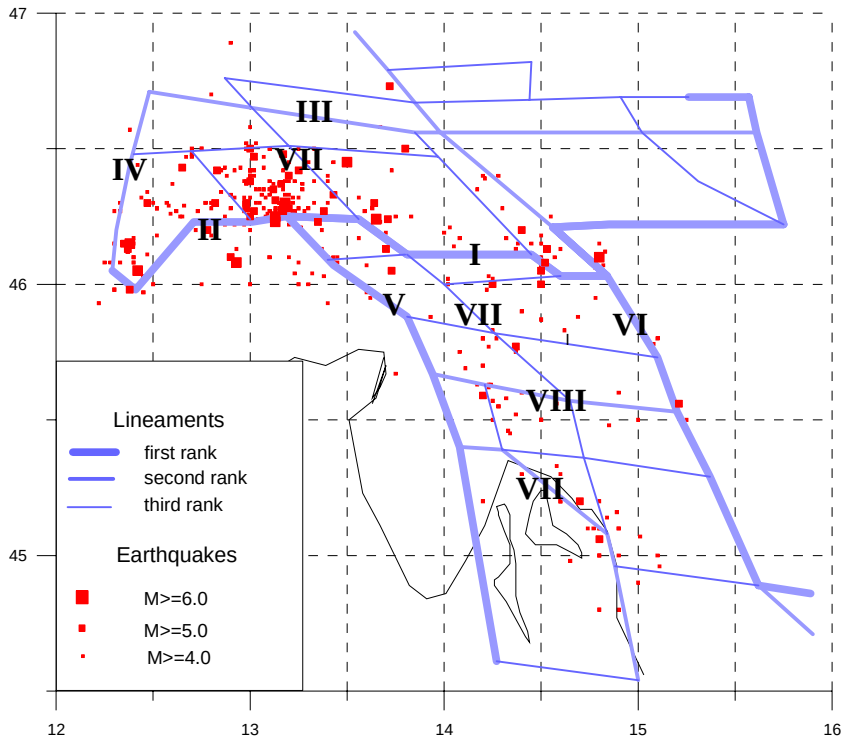


Figure 2.1. Seismicity of the Friuli region (Peresan and Panza. 2002) and the morphostructural zoning (Gorshkov et al., 2004)

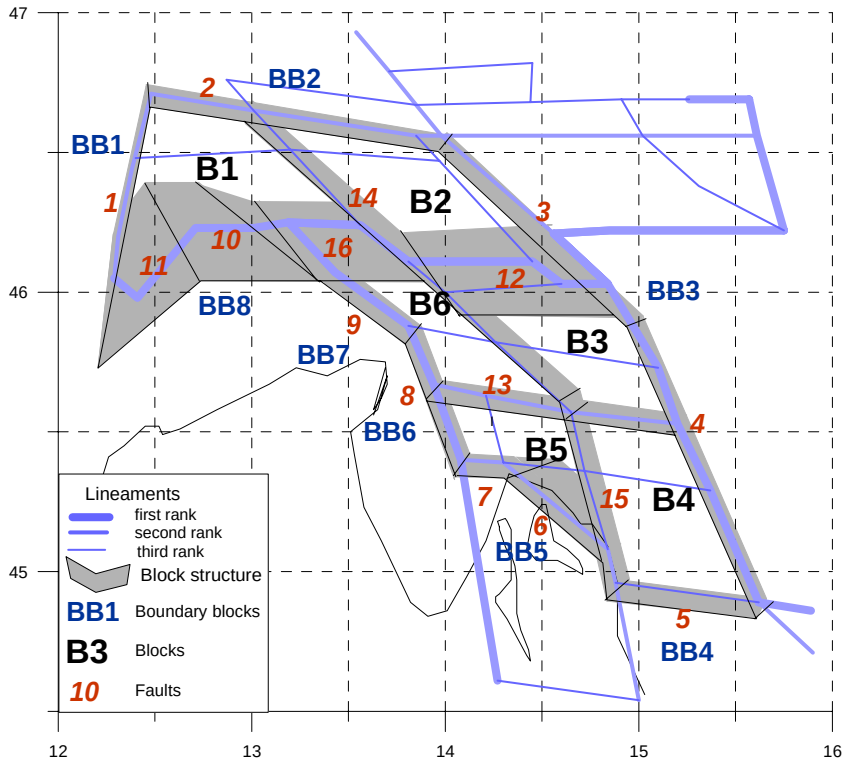


Figure 2.2. Geometry of the block structure outlined on the base of the morphostructural map (Gorshkov et al., 2004)

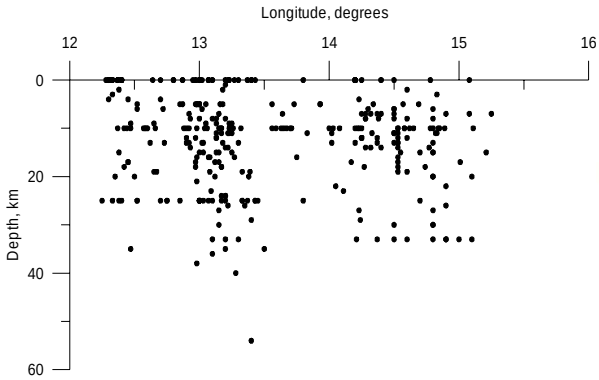


Figure 2.3. Distribution of seismicity in the depth UCI2006 (Peresan and Panza 2002)

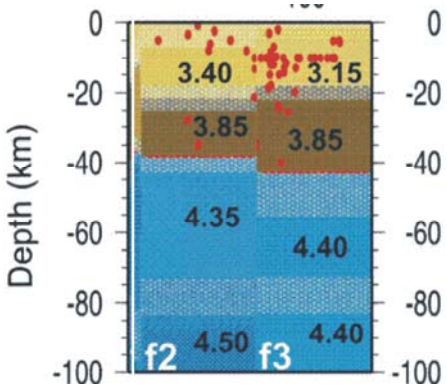


Figure 2.4. Velocities of seismic waves from Structural model of Italy. After Chimera et al.

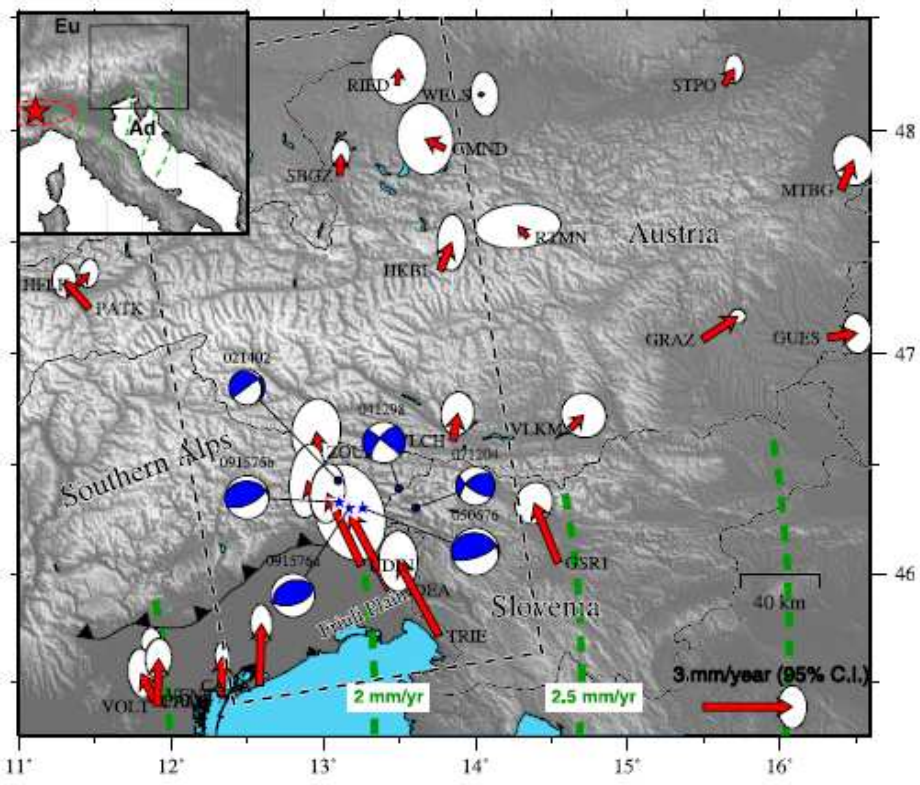


Figure 2.5. The GPS observations. After D'Agostino et al. (2005)

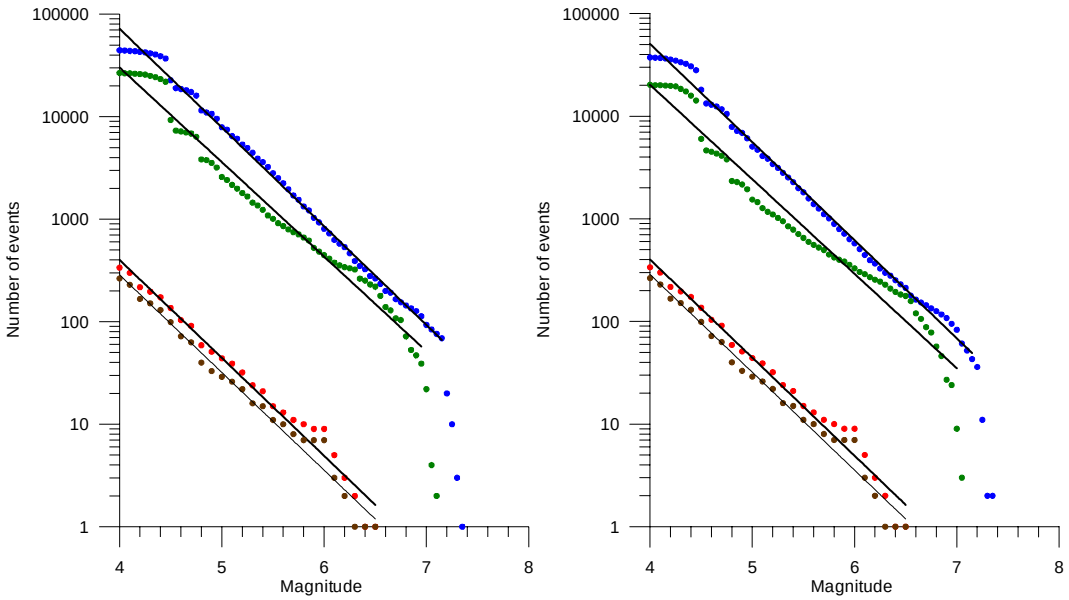


Figure 2.6. Gutenberg-Richter plots for observed and synthetic seismicity: A- prescribed velocity of Adria from whole Italy modeling (Peresan et al., in press); B- prescribed velocity of Adria from GPS observations (D'Agostino et al., 2005)

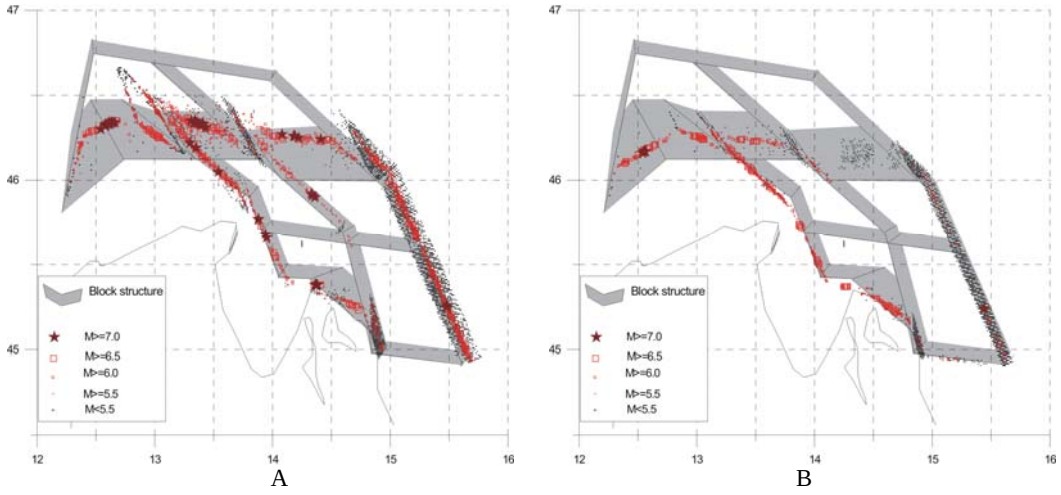


Figure 2.7. Synthetic seismicity, movements from Peresan.et al.(in press), A - depth 40km, B - depth 20km

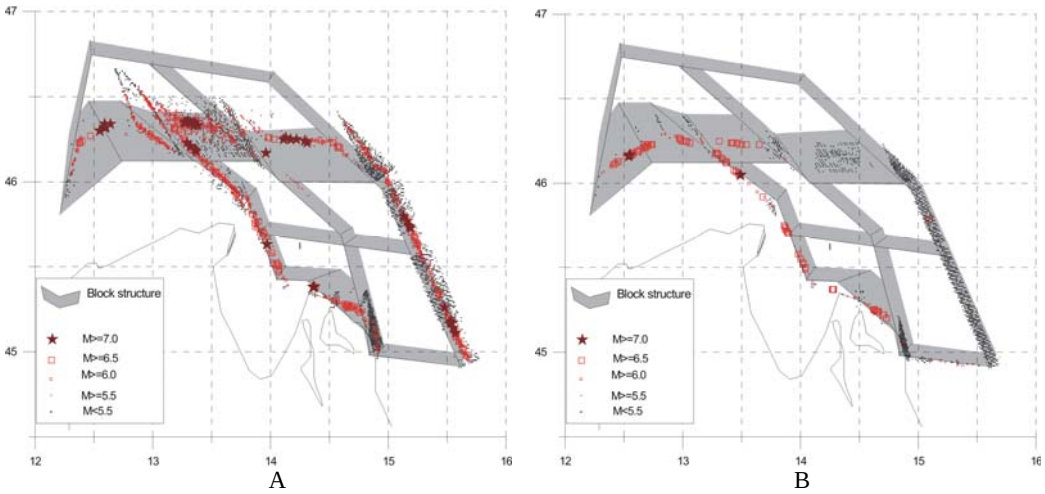


Figure 2.8. Synthetic seismicity, movements from D'Agostino.et al.(2005),A - depth 40km, B-depth 20km


Figure2.9. Identification of seismogenic nodes in the Alps and Dinarides (after Gorshkov et al., 2004). The lines with different thickness represent lineaments of different rank.The red circles indicate the nodes identified to be prone to earthquakes with M≥6.5